The Astrophysical Journal, 831:99 (13pp), 2016 November 1 doi:10.3847/0004-637X/831/1/99

ON UNDERSTANDING THE NATURE OF COLLISIONS OF CORONAL MASS EJECTIONS OBSERVED BY *STEREO*

Wageesh Mishra[1], Yuming Wang[1], and Nandita Srivastava[2,3]
[1] CAS Key Laboratory of Geospace Environment, Department of Geophysics and Planetary Sciences, University of Science and Technology of China, Hefei 230026, China; wageesh@ustc.edu.cn, ymwang@ustc.edu.cn
[2] Udaipur Solar Observatory, Physical Research Laboratory, Badi Road, Udaipur 313001, India
Received 2016 April 18; revised 2016 July 14; accepted 2016 July 22; published 2016 October 28

ABSTRACT

We attempt to understand the collision characteristics of two coronal mass ejections (CMEs) launched successively from the Sun on 2013 October 25. The estimated kinematics, from three-dimensional (3D) reconstruction techniques applied to observations of CMEs by the SECCHI/Coronagraphic (COR) and Heliospheric Imagers, reveal their collision around 37 $R_{\odot}$ from the Sun. In the analysis, we take into account the propagation and expansion speeds, impact direction, and angular size as well as the masses of the CMEs. These parameters are derived from imaging observations, but may suffer from large uncertainties. Therefore, by adopting head-on as well as oblique collision scenarios, we have quantified the range of uncertainties involved in the calculation of the coefficient of restitution for expanding magnetized plasmoids. We show that the large expansion speed of the following CME compared with that of the preceding CME results in a higher probability of super-elastic collision. We also infer that a relative approaching speed of the CMEs lower than the sum of their expansion speeds increases the chance of a super-elastic collision. The analysis under reasonable errors in the observed parameters of the CME reveals a larger probability of occurrence of an inelastic collision for the selected CMEs. We suggest that the collision nature of two CMEs should be discussed in 3D, and the calculated value of the coefficient of restitution may suffer from a large uncertainty.

Key words: Sun: coronal mass ejections (CMEs) – Sun: heliosphere

1. INTRODUCTION

Coronal mass ejections (CMEs), which are the most energetic events on the Sun, are expanding magnetized plasma blobs in the heliosphere. If they reach the Earth with a southward directed magnetic field orientation, they can cause intense geomagnetic storms (Dungey 1961; Gosling 1993; Gonzalez et al. 1994). They are frequently launched from the Sun, especially during solar maximum when their interaction or collision in the heliosphere is possible. Historically, such interaction was inferred using in situ data from *Pioneer 9* and the twin *Helios* spacecraft (Intriligator 1976; Burlaga et al. 1987). However, the first observational evidence was provided by Gopalswamy et al. (2001) using the Large Angle and Spectrometric Choronograph (LASCO; Brueckner et al. 1995) on board the *SOlar and Heliospheric Observatory (SOHO)* and long wavelength radio observations. It has been suggested that some interacting CMEs have a long interval of a strong southward magnetic field and can produce major disturbances in the Earth's magnetosphere (Wang et al. 2003; Farrugia & Berdichevsky 2004; Farrugia et al. 2006; Lugaz & Farrugia 2014).

Before the *Solar TErrestrial RElations Observatory* (*STEREO*) (Kaiser et al. 2008) era, CMEs could only be imaged near the Sun from one viewpoint of *SOHO*, and we lacked three-dimensional (3D) kinematics. Therefore, understanding CME–CME interaction was mainly based on magnetohydrodynamic (MHD) numerical simulation studies (Vandas et al. 1997; Gonzalez-Esparza et al. 2004; Vandas & Odstrcil 2004; Lugaz et al. 2005; Wang et al. 2005; Xiong et al. 2006, 2007, 2009). With the availability of wide angle imaging observations of heliospheric imagers (HIs) on board *STEREO* from multiple viewpoints, several cases of interacting CMEs have been recently reported in the literature (Harrison et al. 2012; Liu et al. 2012; Lugaz et al. 2012; Martínez Oliveros et al. 2012; Möstl et al. 2012; Shen et al. 2012; Temmer et al. 2012; Webb et al. 2013; Mishra & Srivastava 2014; Colaninno & Vourlidas 2015; Mishra et al. 2015a). Also, simulation-based studies on the observed cases of CMEs have also been conducted to advance our understanding of such interactions (Lugaz et al. 2013; Shen et al. 2013, 2014, 2016; Niembro et al. 2015).

Understanding the interaction of CMEs is of interest because of their impact on many areas of heliospheric research. Several cases of CME–CME interaction studies have focused on understanding the nature of their collision, particle acceleration, and geoeffectiveness (Shen et al. 2012; Ding et al. 2014; Lugaz & Farrugia 2014). Interacting CMEs also provide a unique opportunity to study the evolution of the shock strength, structure, and its effect on plasma parameters of preceding CMEs (Wang et al. 2003; Lugaz et al. 2005, 2015; Liu et al. 2012; Möstl et al. 2012). It is suggested that due to preconditioning of the ambient medium by a preceding CME, any following CME may experience high (Temmer et al. 2012; Mishra et al. 2015b) or low drag (Temmer & Nitta 2015) before their noticeable collision or merging. We use the terms "interaction" and "collision" in two different senses as defined in Mishra & Srivastava (2014). By "interaction," we mean a probable exchange of momentum between the CMEs is in progress, however, we could not notice an obvious joining of their features in the imaging observations. "Collision" refers to the scenario noticed in imaging observations, where two CMEs moving with different speeds come in close contact with each other and show an exchange of momentum until they achieve an approximately equal speed or they are separated

[3] Centre for Excellence in Space Sciences, India, http://www.cessi.in.

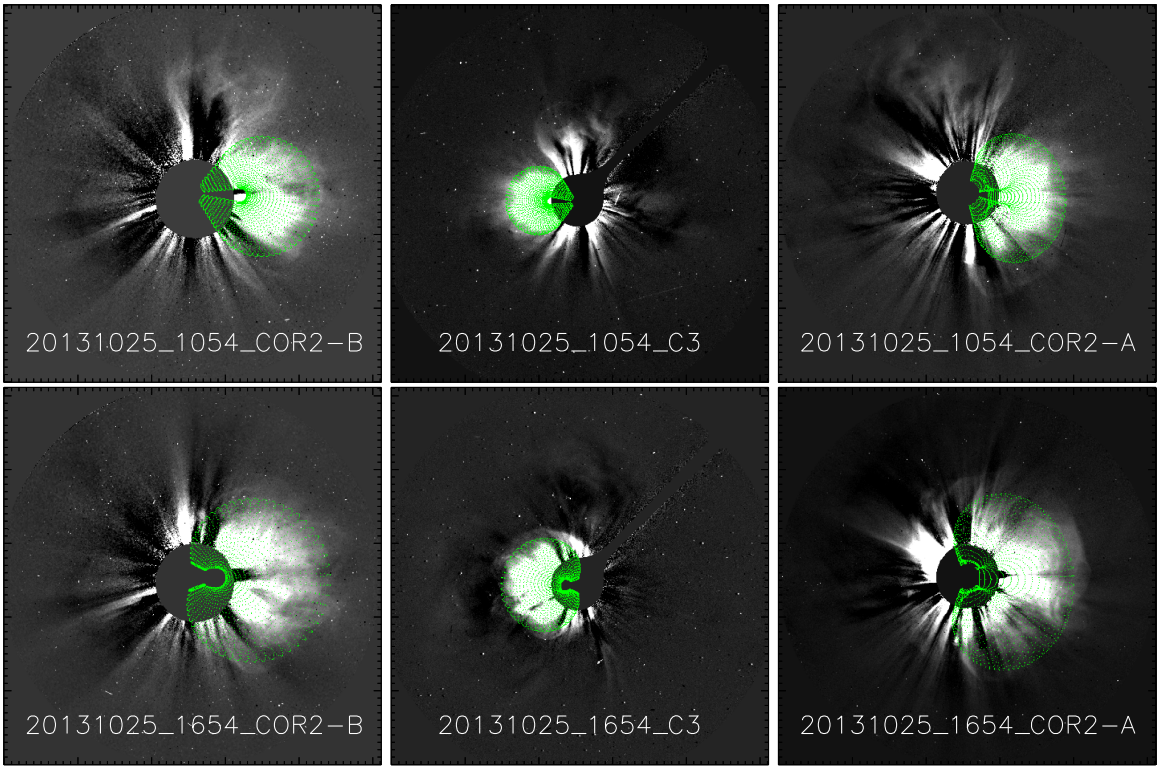

Figure 1. GCS model wire-frame with green overlaid on images of CME1 (top panels) and CME2 (bottom panels). The triplet of concurrent images is taken from *STEREO*/COR2-B (left), *SOHO*/LASCO-C3 (middle), and *STEREO*/COR2-A (right) around 10:54 UT for CME1 and 16:54 UT on October 25 for CME2, respectively.

from each other. Colliding CMEs can display changes in their kinematics and morphology after the collision, and hence the prediction of their arrival time at Earth becomes challenging. Knowledge about the nature of collisions of CMEs may be utilized to predict their post-collision kinematics.

Using twin viewpoint *STEREO* observations, more accurate estimation of the kinematics and the masses of CMEs is possible; however, recent case studies are not in agreement about the nature of CME collisions. This disagreement is possible as each case study has focused on different candidate CMEs likely having different characteristics. Some studies using imaging observations have shown a super-elastic collision of CMEs (Shen et al. 2012; Colaninno & Vourlidas 2015), whereas some advocate inelastic (Mishra et al. 2015a) or close to elastic collision (Mishra & Srivastava 2014; Mishra et al. 2015b). This poses a question as to what determines the nature of collision, i.e., a coefficient of restitution to vary from the super-elastic to the inelastic range. Most of the earlier studies have considered a simplistic approach that CMEs are propagating exactly in the same direction (i.e., head-on collision), and also have not taken the expansion speed or angular size of CMEs into account (Mishra & Srivastava 2014; Mishra et al. 2015a, 2015b). Schmidt & Cargill (2004) have studied obliquely colliding CMEs using numerical simulations. The results of some earlier studies have suggested a collision nature of CMEs based on their deflection and change in the dynamics without explicitly mentioning the value of the coefficient of restitution (Lugaz et al. 2012; Temmer et al. 2012; Colaninno & Vourlidas 2015). For the first time, Shen et al. (2012) studied the oblique collision of CMEs using imaging observations and took several uncertainties into account; however, they did not discuss constraining the conservation of momentum. The straightforward use of observed CME characteristics (speed and mass), which may involve large errors, may be a reason for conservation of momentum to no longer be valid. We admit that previous studies differ from the real scenario and each study has different limitations.

With the exception of Shen et al. (2012), we are not aware of another study that thoroughly addresses the uncertainties involved in understanding the nature of CME collisions. Hence, we take that next step to address the limitations of previous studies and to investigate the role of CME characteristics, e.g., direction, mass, propagation speed, expansion speed, and angular size, on the collision nature. For this purpose, we selected two CMEs that occurred almost 7 hr apart on 2013 October 25 and collided with each other in the HI-1 field of view. A collision around such a moderate distance from the Sun is well suited to our collision picture. This is because near the Sun coronal magnetic structures may interfere with CME dynamics, and accurate estimation of the dynamics far from the Sun using HI observations is difficult (Howard 2011; Davies et al. 2012, 2013; Mishra et al. 2014). We apply the graduated cylindrical shell (GCS) fitting technique (Thernisien et al. 2009) to coronagraphic images and the self-similar expansion (SSE) method (Davies et al. 2012) to HI images of the CMEs to estimate their kinematics. This is discussed in Section 2 including a description of the estimation of the true masses of the CMEs using Colaninno & Vourlidas's (2009) method and identification of the collision phase from the kinematic profile. Section 3 presents the analysis and results from the head-on and oblique collision scenarios and shows the limitations of the approach of a simplistic head-on collision undertaken in previous studies. The various limitations of the present study are discussed in Section 4, and conclusions are presented in Section 5.

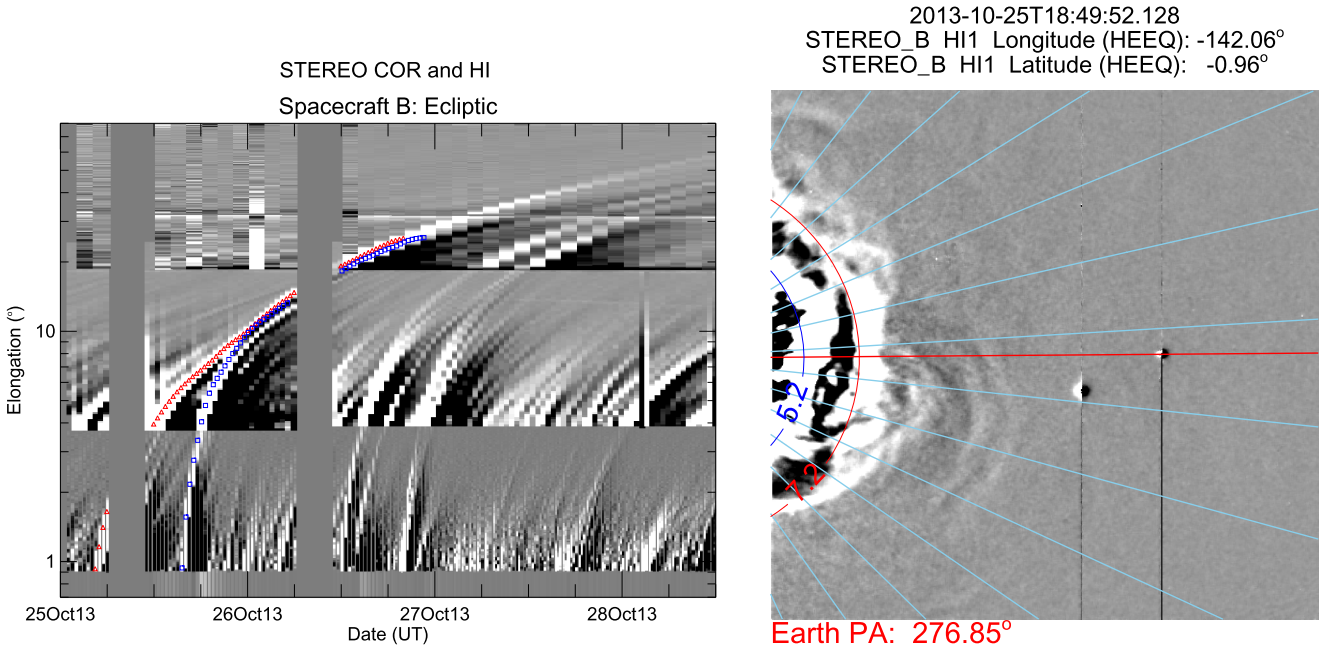

Figure 2. Left panel: time-elongation plot (*J*-map) constructed using COR2-B and HI-B images of *STEREO*/SECCHI Behind spacecraft for the period of October 25–28 at 12:00 UT. The red △ and blue □ mark the evolution of the brightness enhancement (leading edge) due to CME1 and CME2, respectively. Right panel: derived elongation of CMEs at 18:49 UT on October 25 overplotted on HI1-B images.

2. TRACKING OF CMEs IN THE HELIOSPHERE

Tracking of a CME from its lift-off in the corona to the Earth or even beyond is possible using the imaging instruments of the SECCHI package on board the *STEREO* spacecraft. In the following section, we track the heliospheric evolution of CMEs from different viewpoints and apply suitable 3D reconstruction techniques to estimate their kinematics.

2.1. Estimation of Kinematics in the COR2 Field of View

The selected CMEs in our study were recorded as halo CMEs from *SOHO*/LASCO-C2 around 8:15 UT and 15:15 UT on 2013 October 25, respectively. We call these subsequently launched preceding and following CMEs CME1 and CME2, respectively. To estimate the 3D kinematics of CMEs, we have applied the GCS forward-fitting model (Thernisien et al. 2009) to the contemporaneous images of the CMEs obtained from the SECCHI/COR2-B, *SOHO*/LASCO-C3, and SECCHI/COR2-A coronagraphs. Figure 1 shows images of CME1 and CME2 overlaid with the fitted GCS wire-framed contour (in green). From this method, we note the propagation direction of CME1 along E70N03 (within an error of ±5°) at a distance of $11.5 \pm 1.0\ R_{\odot}$. The propagation direction for the following CME2 is along the E65N03 (within an error of ±5°) at a distance of $12.5 \pm 1.0\ R_{\odot}$. In addition to the aforementioned propagation direction, the best visual GCS fitting gives a half angle of 30° ± 5°, a tilt angle of 90° ± 20°, and an aspect ratio of 0.39 ± 0.10 for CME1. The half angle, tilt angle, and aspect ratio for CME2 are 65° ± 5°, 90° ± 20°, and 0.59 ± 0.10, respectively. The 3D speed of CME1 is noted as $485\ \mathrm{km\ s^{-1}}$, and for CME2 it is $1000\ \mathrm{km\ s^{-1}}$. The longitudes of CME1 (i.e., $\phi_1 = -70°$) and CME2 (i.e., $\phi_2 = -65°$) and their speeds suggest their propagation eastward from the Sun–Earth line, and possible interaction or collision at some location in the heliosphere. The aforementioned uncertainties in the GCS fitted parameters are noted by inspecting the differences in the fitted values obtained from several independent attempts of applying the GCS model to the CMEs.

2.2. Estimation of Kinematics in the HI Field of View

Examining the heliospheric evolution of the CMEs, we note that their leading front could not be observed in the HI1-A field of view while their flank remained visible only to a small elongation angle. This is because of largely eastward propagation of the CMEs from the Sun–Earth line. Therefore, we used running difference images of COR2-B and HI-B to construct a *J*-map (Sheeley et al. 1999; Davies et al. 2009) along the ecliptic (left panel of Figure 2). By manually clicking on the positively inclined bright features in the *J*-map that correspond to enhancement of density due to the CMEs, we derived the elongation-time profiles which are shown with red and blue in the figure. We overplotted the derived elongation profile of tracked features to the sequence of HI images, and noted that the features correspond to the leading front of CMEs. For example, the derived elongation angle of CMEs overplotted on an HI1-B image at a particular instant is shown in the right panel of Figure 2. We confirm that tracked leading edges of the CMEs meet around a 10° elongation. Based on our earlier study on the comparison of the relative performance of reconstruction methods (Mishra et al. 2014), we implement the SSE reconstruction method developed by Davies et al. (2012). This method requires the propagation direction of the CME and an input of cross-sectional angular half-width (λ) of the CME fixed to an appropriate value. Based on the formulation described in the appendix of Mishra et al. (2015b), we used the GCS fitted parameters and found the values of λ for the CMEs. The calculated value of λ for CME2 is around 35 ± 5°, which is almost 10° larger than its value for CME1. The values of λ for CME1 and CME2 as of 25° and 35° are used as input while implementing the SSE method. However, we acknowledge the errors in the calculation of λ, and to examine its effect on the kinematics of the CMEs (Mishra

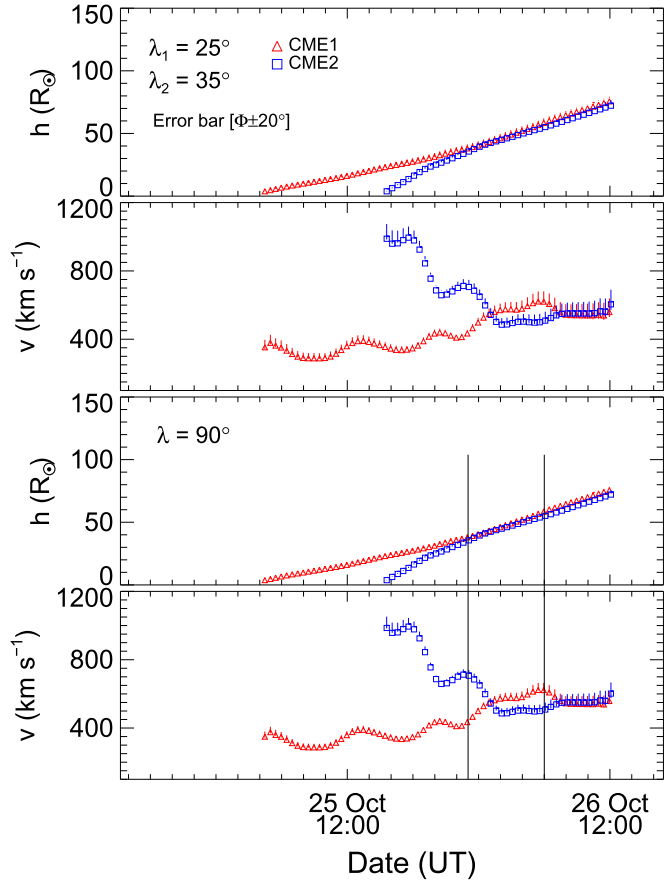

Figure 3. From the top: the first and second panels show time variation of the height and speed of the leading edge of the 2013 October 25 CMEs from the SSE method. The third and fourth panels show the variation of height and speed from the HM method. The vertical dashed lines in the bottom panels mark the start and end of the collision phase. The small vertical line at each data point is the error bar due to an uncertainty of ±20° considered in the value of propagation direction estimated from the GCS model.

et al. 2015b), we also implement the harmonic mean (HM) method of Lugaz et al. (2009), which is equivalent to the SSE method with $\lambda = 90°$. The derived elongation profile from *J*-map is interpolated keeping a half hour interval to get kinematics data points closely connected. The estimated kinematics are shown in Figure 3. The two upper and two lower panels in the figure show the kinematics from the SSE and HM methods, respectively. The speed is estimated from adjacent distance points using a numerical differentiation with a three-point Lagrangian interpolation and therefore have misleading nonphysical fluctuations. The smooth profile of speed can be derived by fitting the distance into a polynomial, but the information about short time variations in the speed during CME–CME interaction will also be lost. Despite having nonphysical fluctuations in the speed, a careful inspection of the height–time tracks, together with the speed profiles, helps to mark the timing for the CMEs coming into close contact with one another for the collision.

Although we have taken extreme care in manual tracking, we acknowledge the possibility of error (≈2°) in elongation measurements from the *J*-map. Based on our earlier study (Mishra et al. 2015b), we note that an error of around 2° in elongation has less of an effect on the kinematics than an error of around 10° in the propagation direction of the CMEs. The error in the estimated direction of the CMEs from the GCS method is around 5° in the COR field of view. However, the collision leading to a possibility of their real deflection (Lugaz et al. 2012) may increase the error in the direction in the HI field of view where the collision takes place. The effect of real or artificial deflection (Howard & Tappin 2009; Howard 2011) of CMEs on the estimated kinematics may be crucial. To find the maximum possible error in kinematics induced from uncertainties in direction, a change of ±20° in the propagation direction of the CMEs is considered in our study. We note that such a change in direction shows only a small effect on the kinematics at smaller elongation, as has been reported previously (Wood et al. 2010; Howard 2011; Mishra et al. 2014). From the obtained kinematics, we notice that a change in λ value for the selected CMEs also has a small effect on the kinematics obtained from the SSE method. This supports the findings of earlier studies which have shown that a change in the value of λ significantly alters the kinematics of only those CMEs that are propagating more than 90° away from the Sun–observer line (Liu et al. 2013; Mishra et al. 2015b; Vemareddy & Mishra 2015). The kinematics at higher elongations are truncated where they have large fluctuations primarily because of large errors in tracking the CMEs and hence elongation measurements from the *J*-map. Identifying the collision phase as described in Mishra et al. (2015b), we notice that collision begins on October 25 at 23:00 UT and ends on October 26 at 06:00 UT. We emphasize that the timings for collision are based on the exchange of momentum between both the CMEs revealed from estimated kinematics of their leading edges. However, the leading edge of CME2 meets the trailing edge of CME1 before the observed time of acceleration of the leading edge of CME1. As the signal transferring the momentum had to travel from the trailing edge of CME1 to its leading edge, the time for the beginning of collision noted above is delayed more than the actual starting time of the interaction between the CMEs. If the signal is carried by magnetohydrodynamic waves, the spatial length and plasma properties of CME1 will decide the time taken by the signal during its journey from the trailing edge to the leading edge of CME1. Thus, the precise start and end of the momentum exchange between the CMEs is difficult to mark. We note that during the collision phase of around 7 hr, CME1 accelerated from $u_1 = 425$ to $v_1 = 625\,\mathrm{km\,s^{-1}}$ and CME2 decelerated from $u_2 = 700$ to $v_2 = 500\,\mathrm{km\,s^{-1}}$. The true masses of the both the CMEs are determined using COR2 images, following the method of Colaninno & Vourlidas (2009). The masses of CME1 and CME2 are estimated to be 7.5×10^{12} kg and 9.3×10^{12} kg, respectively. At the beginning of the collision, the CME2 leading edge is around 37 $R_\odot$, whereas it is around 58 $R_\odot$ at the end of the collision phase.

3. COEFFICIENT OF RESTITUTION FOR THE CMEs: ANALYSIS AND RESULTS

In this section, first we estimate Newton's coefficient of restitution (Newton 1687) for the colliding CMEs following the treatment of head-on collision as described in Mishra & Srivastava (2014) and Mishra et al. (2015a). Then we consider a more realistic scenario of oblique collision. As the selected CMEs are propagating along the same latitude, almost in the ecliptic along which the *J*-map is made, therefore Figure 3 represents the kinematics of only a portion of the CME moving in a two-dimensional (2D) plane. This indicates that our consideration of head-on and oblique collisions stand for

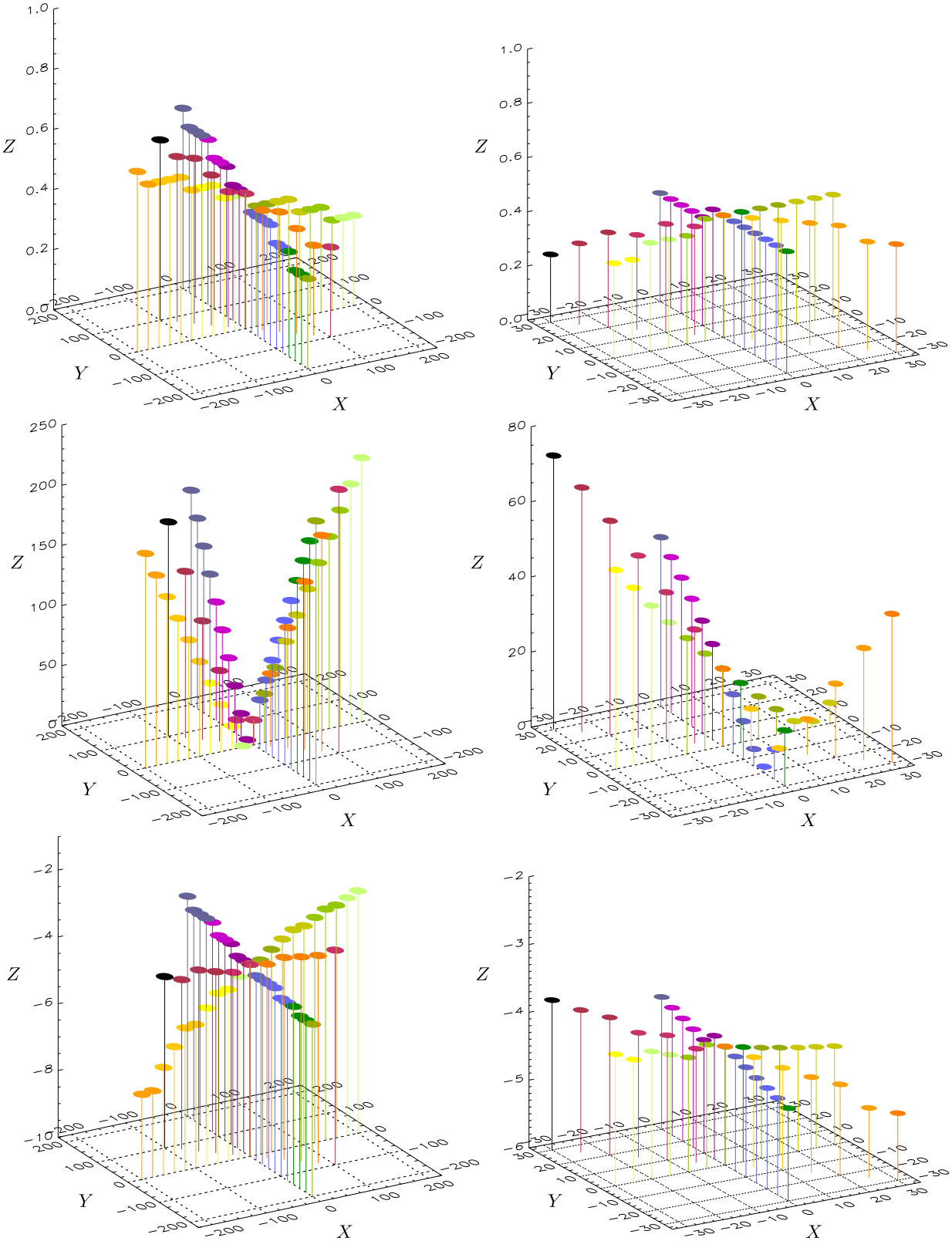

Figure 4. The Z axis in top, middle, and bottom panels stands for the coefficient of restitution (e), deviation in observed speed (σ), and change in total kinetic energy of the CMEs, respectively. In the left panels: the X axis and Y axis, respectively, show the uncertainties of ± 200 km s^{-1} in the observed pre-collision speeds (u_1, u_2) and post-collision speeds (v_1, v_2) of the CMEs. The different parameters shown on the Z axis in different panels with the same colors correspond to equal uncertainties in observed speeds. In the right panels: the X and Y axes represent the $\pm 30\%$ uncertainties in the estimated masses of CME1 and CME2, respectively. The different parameters shown on the Z-axis in different panels with the same color correspond to the equal uncertainties in the observed mass of the CMEs.

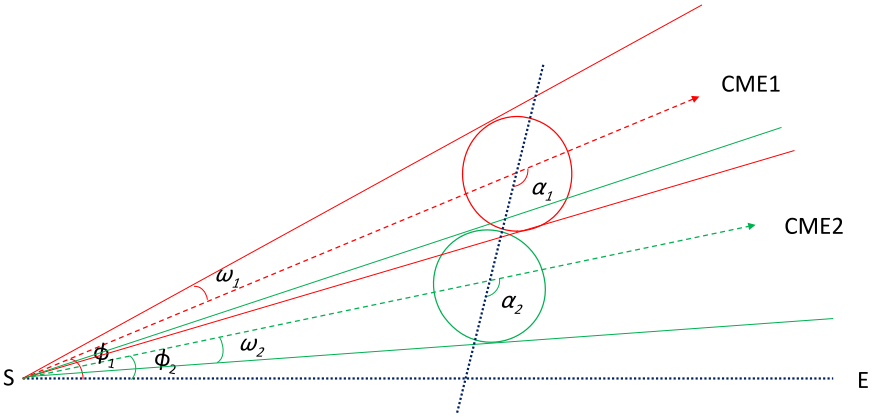

Figure 5. Oblique collision of two CMEs assumed as spherical bubbles. The red and green circles represent the preceding CME1 and the following CME2. The dotted horizontal line marks the Sun–Earth line, and the dotted oblique line is passing through the centroid of both CMEs. The dashed red and green lines show the directions of propagation (i.e., longitude) of CME1 and CME2 as ϕ_1 and ϕ_2 from the Sun–Earth line, respectively. ω_1 and ω_2 are the half-angular width of CME1 and CME2, respectively. α_1 and α_2 are the directions of propagation of CME1 and CME2 from the line joining their centroid.

the 1D and 2D collision pictures. Putting together the results of the analysis for the 1D and 2D pictures helps us to realize several interesting points that must be addressed for improving our understanding of the collision nature of any magnetized and expanding plasma blobs, such as CMEs.

3.1. Head-on Collision Scenario

In this scenario, we assume that the directions of both the CMEs before and after the collision are roughly the same. We then modify the observed post-collision speeds (v_1, v_2) of the CMEs to satisfy the conservation law of momentum. At the same time, we minimize the deviation (σ) between the modified and observed post-collision speeds. We call the modified speeds theoretically estimated post-collision speeds ($v_{1\mathrm{th}}$, $v_{2\mathrm{th}}$) and define the deviation as $\sigma = \sqrt{[(v_{1\mathrm{th}} - v_1)^2 + (v_{2\mathrm{th}} - v_2)^2]/2}$. We find that the most optimized theoretically estimated post-collision speeds of CME1 and CME2 are 645 and 520 km s^{-1}, respectively, with $\sigma = 20$ km s^{-1}. Thus, adopting the head-on collision and constraining the conservation of momentum, the coefficient of restitution (e) is estimated to be about 0.45, suggesting an inelastic nature of collision. The total kinetic energy before the collision was 2.95 $\times$ 10^{24} J, which decreased by ≈4.2% for the derived value of $e = 0.45$. The kinetic energy of CME1 and CME2 before the collision was 6.8 $\times$ 10^{23} J and 2.27 $\times$ 10^{24} J, respectively. After the collision, the kinetic energy of CME1 increased by 130%, whereas the kinetic energy of CME2 decreased by 44.5% of its value before the collision.

There is a possibility of error in the estimated speeds (Lugaz et al. 2009; Davies et al. 2012) and the masses of the CMEs (Colaninno & Vourlidas 2009). Therefore, to examine their effect on the nature of collision, we consider an arbitrary uncertainty in speed by ±200 km s^{-1} and in mass by 30%. Without considering the expansion speeds of the CMEs, an uncertainty in their leading edge speeds is chosen such that they satisfy the 1D collision condition, i.e., $u_2 \geqslant u_1$, $v_1 \geqslant u_1$ and $v_2 \leqslant u_2$. The results of the estimated value of e, kinetic energy change, and value of σ is shown in Figure 4. The Z-axis in the top, middle, and bottom panels represents the values of e, σ, and the change in total kinetic energy of the CMEs. The X and Y axes in the left panels represent the uncertainties in observed pre-collision and post-collision speeds of the CMEs, whereas in the right panels they represent the uncertainties of ±30% in the measured masses of CME1 and CME2, respectively. From the figure, we can note that an error of ±100 km s^{-1} in the observed speeds can result in variation of the coefficient of restitution from 0.3 to 0.6 with deviation (σ) values up to 200 km s^{-1}. We point out that while examining the effect of uncertainties, the speed of CMEs with uncertainties is now considered the observed speed and then their post-collision speed is modified for conservation of momentum with a minimum value of deviation. Corresponding to an uncertainty of ±100 km s^{-1} in speeds, the total kinetic energy of the CMEs decreases by 3.5%–5.7% of its value before the collision.

The value of e corresponding to larger uncertainties in speed and mass leading to a higher value of σ is less reliable. This is because a large σ suggests that the theoretically estimated observed speed satisfying the condition for conservation of momentum is significantly different than the observed speed of the CMEs. From the bottom panels, interestingly we note that ±30% in the masses of the CMEs gives a small change in the value of e from 0.25 to 0.45 with a small value of σ up to 75 km s^{-1}. Such findings suggest that even a large error in the mass estimates of the CMEs does not impose a lack of certitude on our estimated e value, i.e., the nature of collision. The uncertainty in speeds may indirectly arise from the errors in direction, expansion speed, and angular width of the CMEs. Hence the influence of these factors on the nature of the collision must be discussed.

3.2. Oblique Collision Scenario

For a realistic situation close to the observations, we include the possibility of an oblique CME collision with certain angular widths. We consider CME1 and CME2 as expanding spherical bubbles propagating in the ϕ_1 and ϕ_2 directions relative to a common reference line (i.e., the Sun–Earth line in this case) with angular sizes of ω_1 and ω_2, respectively (Figure 5). We consider that the centroids of CME1 and CME2 are propagating in the direction α_1 and α_2 relative to the line joining their centroids at the instant of collision.

Using reconstruction methods described in Section 2.1, we have estimated ϕ_1 and ϕ_2 and now calculate α_1 and α_2 using

the following relation.

$$\cos(|\phi_1 - \phi_2|)\sin(\alpha_1) + \sin(|\phi_1 - \phi_2|)\cos(\alpha_1) = \frac{\sin(|\phi_1 - \phi_2|) - \sin(\omega_2)\sin(\alpha_1)}{\sin(\omega_1)}$$
$$\alpha_2 = \alpha_1 + |\phi_1 - \phi_2|. \quad (1)$$

We have estimated the speed of the leading edge of the CMEs, however, the speed of their centroids should be used to discuss the collision nature. Hence, the pre-collision speed of the centroid for CME1 will be $u_{1c} = u_1 - u_{1ex}$, where u_1 is the leading edge speed, and u_{1ex} is the expansion speed of CME1. By assuming that the CME expands in such a way as to keep its angular width constant, we get $u_{1ex} = u_1 \sin(\omega_1)/[1 + \sin(\omega_1)]$. Similarly, the centroid speed of CME2 (u_{2c}) is equal to the difference between its leading edge speed (u_2) and expansion speed (u_{2ex}). We consider that the post-collision direction of propagation of the CMEs relative to the Sun–Earth line is ϕ_1' and ϕ_2', and relative to the line joining their centroid it is $\beta 1$ and $\beta 2$. The post-collision speeds of the centroids of CME1 and CME2 are v_{1c} and v_{2c}, respectively. We note that due to the presence of the errors in observed pre- and post-collision speeds they are not necessarily satisfying the momentum conservation. Also, during the collision, if there is a deflection of the CMEs then their observed post-collision dynamics (Figure 3) will be modified and its magnitude will also depend on the nature of the collision. Hence, the observed post-collision dynamics cannot be used directly to study the nature of collision. Therefore, we determined theoretically the post-collision speeds (v_{1cth}, v_{2cth}) of the centroids of the CMEs using a certain value for e, which together allows the momentum to be conserved. Equation (2) is used for the speed (i.e., $v_{cth}\cos(\beta)$) of the CMEs parallel to the line joining their centroid. Under the collision scenario, an exchange of momentum takes place only along the line joining the centroids of the CMEs and therefore, their speeds perpendicular to that line remain equal before and after the collision. Equation (3) represents this condition mathematically for both the CMEs.

$$v_{1cth}\cos(\beta_1) = \frac{m_1u_1\cos(\alpha_1) + m_2u_2\cos(\alpha_2) - m_2e[u_1\cos(\alpha_1) - u_2\cos(\alpha_2)]}{m_1 + m_2}$$
$$v_{2cth}\cos(\beta_2) = \frac{m_1u_1\cos(\alpha_1) + m_2u_2\cos(\alpha_2) + m_1e[u_1\cos(\alpha_1) - u_2\cos(\alpha_2)]}{m_1 + m_2} \quad (2)$$

$$u_{1c}\sin(\alpha_1) = v_{1cth}\sin(\beta_1)$$
$$u_{2c}\sin(\alpha_2) = v_{2cth}\sin(\beta_2). \quad (3)$$

Using Equations (2) and (3), we determined the post-collision directions (β_1 and β_2) of the CMEs and their post-collision speeds (v_{1cth} and v_{2cth}) along these directions by choosing a set value of the coefficient of restitution (e). Considering that the angular size of the CMEs remains unchanged before and after the collision, v_{1cth}, v_{2cth} are converted to post-collision leading edge speed (v_{1th}, v_{2th}) which is compared with the leading edge speed (v_1, v_2) as observed using HI-1 data. We repeat the abovementioned procedures and calculate a set of theoretical values of final speed (v_{1th}, v_{2th}) corresponding to different values of e. The best suited value of e is attributed to the nature of collision of the selected CMEs for which the deviation (i.e., σ as defined in Section 3.1) between the observed and the theoretically estimated post-collision leading edge speed is minimum. In our study, we have also estimated the post-collision direction of the CMEs ϕ_1' and ϕ_2' to measure the deflection of the colliding CMEs from the Sun–Earth line.

From the above description, it is clear that deflection of the CMEs during their collision has not been taken into consideration to derive their position and speed from the SSE method. This is because the post-collision directions in our approach are found for a certain value of the coefficient of restitution, and hence both are interrelated as we have five unknown parameters and four equations (Equations (2) and (3)) to deal with. By defining a parameter as variance (σ), we could manage to obtain the most likely value of e and thus all five unknown parameters. The values of the observed post-collision speeds from the reconstruction methods (SSE and HM) are not directly used in our analysis. If the deflection of CMEs could have been estimated independently of any collision parameters, such as using elongation measurements and fitting methods (Rouillard et al. 2008), then we would have taken this deflection into account while implementing the SSE method for estimation of kinematics. However, we have used the estimated value of deflection for the CMEs to find their theoretical post-collision speeds. The theoretically estimated post-collision directions and speeds suggest that the deflection of the CMEs are indirectly taken into account for analyzing the collision picture. For the selected CMEs, we estimated the coefficient of restitution (e) in the oblique collision scenario using the estimated kinematics and angular width of the CMEs (Section 2.2). From this, the value of e is estimated to be 0.6 for a 2D collision scenario. This leads to a 3.3% decrease in the total kinetic energy of the CMEs. The value of e from the 2D scenario is almost equal to the value of e estimated for a 1D collision scenario without taking into account the uncertainties in the speeds and masses of the CMEs. This finding is expected as the propagation directions of CME1 and CME2 are only 10° different from each other. Therefore, it will be interesting to see the value of e in the 2D scenario by taking different propagation directions for the CMEs.

3.2.1. Effect of Propagation Direction

The collision takes place in the HI field of view where a larger uncertainty in direction is possible than that in the COR field of view. To examine the role of direction in our analysis, we consider an uncertainty of ±20° in the estimated longitudes of CME1 and CME2 (ϕ_1 and ϕ_2) from the GCS model described in Section 2.1. Then we followed the procedures described in Section 3.2 to calculate the coefficient of restitution and deviation in the speed, which is shown in Figure 6. Only those pairs of directions for the CMEs are chosen for which the collision condition is satisfied. The condition is that the speed of the leading edge of CME2 should be greater than or equal to the speed of the trailing edge of CME1 along the line joining their centroids, i.e., $[u_{2c}\cos(\alpha_2) + u_{2ex}] \geqslant [u_{1c}\cos(\alpha_1) - u_{1ex}]$, and the separation angle between the CMEs should be less than or equal to the sum of their angular sizes, i.e., $|\phi_1 - \phi_2| \leqslant (\omega_1 + \omega_2)$. The left and middle panels of Figure 6 have missing values at the top left and bottom right corners where the longitudes of the CMEs do not satisfy the collision condition. From the figure, we see that the value of e is less than unity in the region bounded between two white dashed lines. There are instances

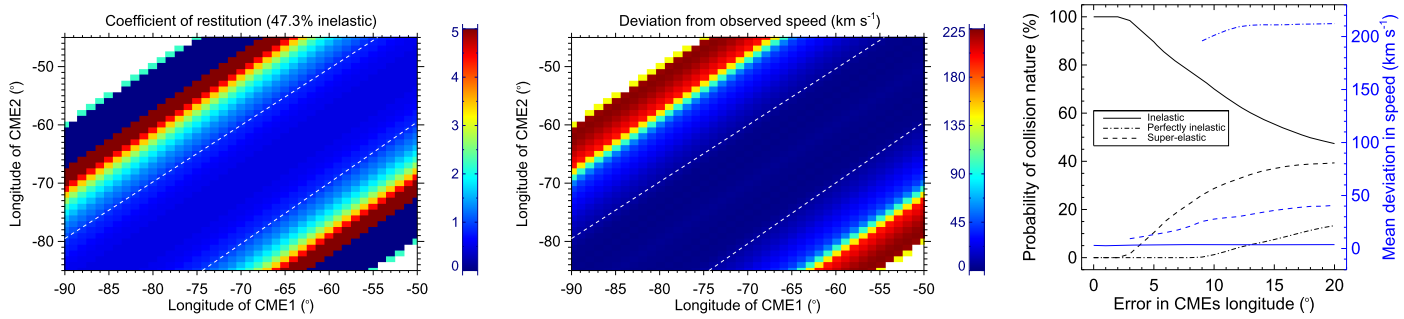

Figure 6. The left and middle panels show the coefficient of restitution (e) and corresponding deviation (σ) between theoretical and observed post-collision speed values. The pre-collision longitudes of CME1 and CME2 are shown on the X and Y axes. The white dashed lines bound the region where nature of collision is inelastic, i.e., $e < 1$. The color bar showing the range of the values shown in the figures is also stacked. The right panel shows the probability of the nature of collision and mean deviation in the speed with error in CME longitude.

near the top left and bottom right corners where the value of e is either equal to zero or greater than unity. The large σ value at these corners corresponding to a large separation angle between the CMEs suggests less reliability of the e value there. Therefore, there is a higher probability of an inelastic nature of collision for the 2013 October 25 CMEs.

In the right panel, we show the probability of the collision nature on the Y axis on the left and the mean value of deviation in the speed on the Y axis on the right, against the error in the CME longitudes on the X axis. This shows that when error in longitude increases from $\pm 1°$ to $\pm\ 20°$, the probability of inelastic collision decreases from 100% to 47.3% with mean deviation always less than $10\,\mathrm{km\,s^{-1}}$. The probability is calculated based on the number of data points created using the pair of CMEs directions. The increasing errors in the longitude increase the probability of a super-elastic nature of collision from 0% to 40% and mean deviation in speed from 10 to $50\,\mathrm{km\,s^{-1}}$. We also infer that the observed collision can never be attributed as perfectly inelastic because an extremely large value of mean deviation in speed is required to make that happen. This emphasizes the difference in results from head-on and oblique collision scenarios. We accept the limitations of previous studies (Mishra & Srivastava 2014; Mishra et al. 2015a) where only the head-on collision is adopted. We note that the range of e values for an inelastic collision nature give the decrease in kinetic energy of the CMEs up to 4% and super-elastic collision nature result in an increase in the kinetic energy of the CMEs up to 15% of its value before the collision.

It is noted that an error in the direction of the CMEs can result in a different value of e using our approach, probably because of erroneously using the value of speed in our analysis. Hence, the estimated value of e with a larger value of σ is reasonably less reliable. We consider the longitude of the CMEs propagating east and west of the Sun–Earth line with negative and positive signs, respectively. The post-collision longitude of the CMEs is $\phi' = \phi + (\beta - \alpha)$ for $\phi_1 < \phi_2$ and $\phi' = \phi - (\beta - \alpha)$ for $\phi_1 > \phi_2$. We note that collision causes the deflection of both CMEs up to $\pm 15°$ in the direction opposite to each other and therefore post-collision angular separation between the CMEs is larger than its pre-collision value. There is a probability of 80% that the deflection of CME2 is 0.5–0.7 times that of the CME1 deflection, and this is reasonable as CME2 is heavier than CME1. The deflection for the interacting CMEs of 2010 May 23–24 has been pointed out by Lugaz et al. (2012). From our analysis, it seems that the uncertainty in the directions of selected colliding CMEs have only a pseudo-effect on the collision nature. We use the term "pseudo" because the use of different directions may cause the alteration in the value of e which mistakenly would be believed if the larger value of σ is overlooked. The larger value of σ implies that the unreliable value of e is due to using the kinematics which does not represent the observed collision picture. Such a dubious effect on the estimated e value is possible because of the errors in ϕ and use of the observed speed estimated along different values of ϕ.

3.2.2. Effect of Angular Size

We further examine the nature of collision of the CMEs because of uncertainty in their angular sizes. The large angular size of the CME directly implies a large value of expansion speed and therefore smaller speed of CME centroid, keeping its leading edge speed as constant. Keeping the kinematics the same as estimated in Section 2, we arbitrary take the angular width ranging between 5° and 35° and repeat the procedures described in Section 3.2. The estimated values of e and σ are shown in the left and right panels of Figure 7. Despite having large uncertainty in the angular size, the probability of an inelastic nature of collision is around 75.6%. The deflection of both the CMEs is up to $\pm 10°$ in the direction opposite to each other because of their collision.

From the figure, it is clear that at the top left corner, the value of e is greater than unity and represents a super-elastic nature of collision. The value of e shown in Figure 7 for a super-elastic nature of collision corresponds to an increase in kinetic energy of the CMEs up to 6%, and for inelastic collision nature corresponds to a decrease in kinetic energy up to 12% of its value before the collision. Around 99% of data points for the super-elastic nature of collision show that the angular width of CME2 is more than 1.5 times that of the CME1 width. Corresponding to this, the expansion speed of CME2 is more than or equal to 2.0 times the CME1 expansion speed. The value of σ for the super-elastic collision nature ranges from 5 to $50\,\mathrm{km\,s^{-1}}$ which is not larger than its value for the inelastic nature of collision. The values of e equal to zero in the bottom right corner of the left panel of the figure are associated with a CME1 expansion speed that is more than 1.5 times that of the expansion speed of CME2. This suggests that a super-elastic nature of collision is probable with a larger expansion speed of the following CME.

Using the expansion speed corresponding to different angular sizes of the CMEs, we determined the speed of their centroids, i.e., u_{1c} and u_{2c}. As per the suggestion made in Shen et al.

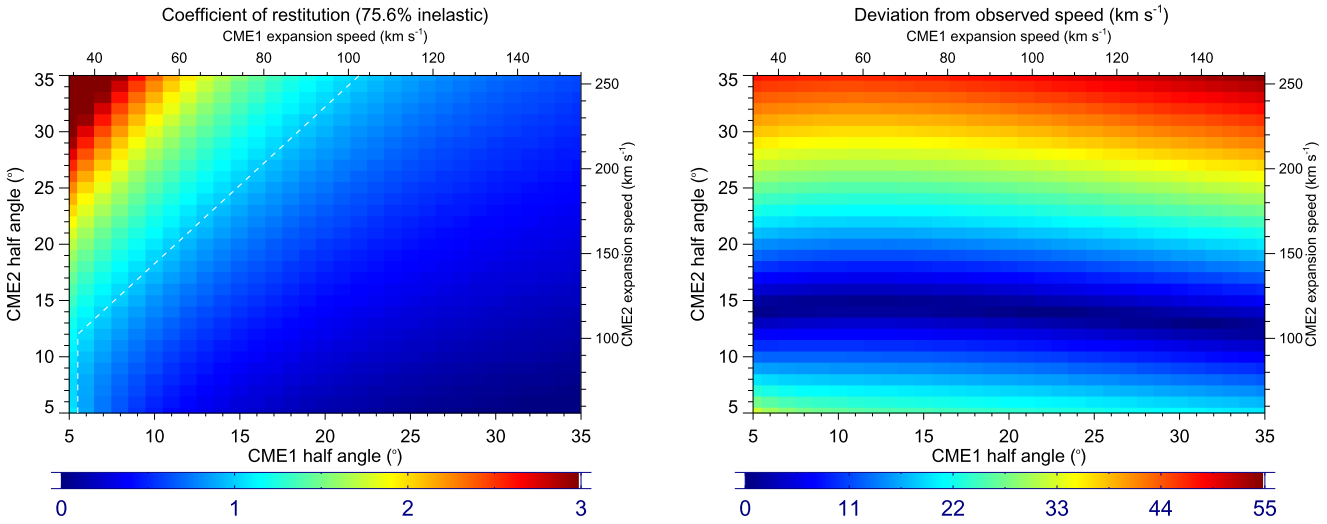

Figure 7. The left and right panels show the coefficient of restitution (e) and corresponding deviation (σ) between theoretical and observed post-collision speeds. Conventional X and Y axes represent the half angles (ω) of CME1 and CME2, respectively. The X and Y axis at the top and right sides, respectively, show the expansion speeds of CME1 and CME2. The dashed white line marks the boundary of the super-elastic and inelastic regimes. The color bar is stacked below the X axis of the figure.

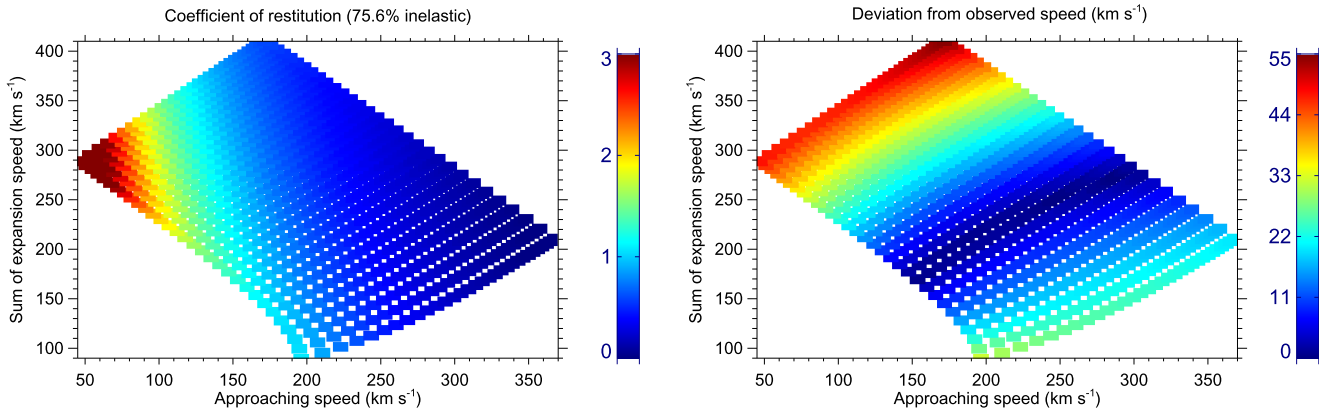

Figure 8. The left and right panels show the coefficient of restitution (e) and corresponding deviation (σ) between the theoretical and observed post-collision speeds. The X axis represents the relative approaching speed of the CMEs, i.e., $[u_{2c}\cos(\alpha_2) - u_{1c}\cos(\alpha_1)]$. The sum of the expansion speeds of CME1 and CME2, i.e., $u_{1ex} + u_{2ex}$, is shown along the Y axis. The color bar is stacked to the right of the figure.

(2012), we examined the characteristic of collision with the approaching speed of the CMEs ($|u_{2c}\cos(\alpha_2) - u_{1c}\cos(\alpha_1)|$) and the sum of their expansion speeds before the collision. Figure 8 (left) shows the variation in e value against their relative approaching speeds on the X axis and the sum of their expansion speeds on the Y axis. From the figure, it is clear that the nature of collision is found to be super-elastic when the sum of the expansion speed is equal to or larger than the relative approaching speeds of the two CMEs before the collision. This finding is consistent with the condition for super-elastic collision conceptualized in Shen et al. (2012, 2016). However, this appears only as a necessary condition but not a sufficient condition for a super-elastic collision. Among all the values of e for an inelastic collision nature, around 63% of them also satisfy this condition. For the selected CMEs under the assumed uncertainties in the half-angular width, we note that almost 99% of the data points for an inelastic nature of collision correspond to a CME2 expansion speed ranging between around 0.3 and 2.5 times that of the CME1 expansion speed. In contrast, the expansion speed of CME2 ranges between around 2 and 7 times that of the CME1 expansion speed for a super-elastic collision.

The value of σ corresponding to the estimated value of e is shown in Figure 8 (right). In this figure, unlike the case shown in Figure 6, we note that the value of σ corresponding to a super-elastic nature of collision is not larger than its value for an inelastic collision nature. Therefore, the estimated value of e for a super-elastic collision is reliable in this case. For the selected CMEs, under the assumed uncertainties in their angular size, the ratio of CME2 to CME1 expansion speed as 2.0 or the low approaching speed around 150 km s^{-1} is a threshold to turn on the super-elastic nature of collision. The larger expansion speed of CME2 compared with that of CME1 and the lower approaching speed appear to be two important conditions for increasing the probability of a super-elastic collision. Both conditions support each other as an increase in the expansion speed of CME2 indirectly gives a lower value of relative approaching speed of CME1 and CME2 than the sum of their expansion speeds.

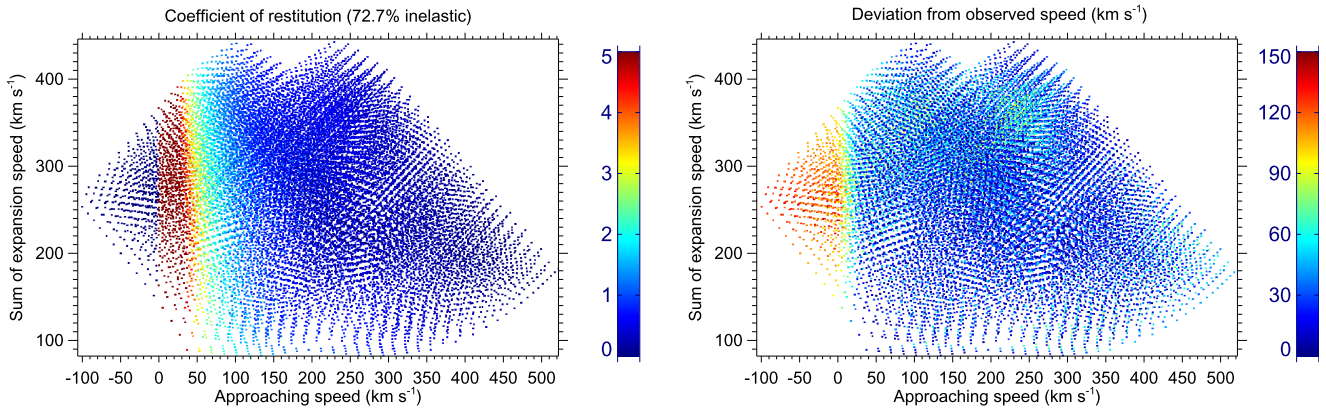

Figure 9. The left and right panels show the coefficient of restitution (e) and corresponding deviation (σ) between theoretical and observed post-collision speeds. The X axis represents the relative approaching speed of the CMEs, i.e., $[u_{2c}\cos(\alpha_2) - u_{1c}\cos(\alpha_1)]$. The sum of the expansion speeds of CME1 and CME2, i.e., $u_{1ex} + u_{2ex}$, is shown along the Y axis. The color bar is stacked to the right of the figure.

3.2.3. Effect of Initial Speed and Angular Size

We further consider the uncertainties of $\pm 100\,\mathrm{km\,s^{-1}}$ in the observed pre-collision leading edge speed (u_1 and u_2) of the CMEs together with uncertainties in their angular width (ω_1 and ω_2). The longitudes of the CME1 and CME2 are taken as estimated using the GCS model of 3D reconstruction in Section 2.1 and the angular width of the CMEs is considered to range from 5° to 35°. We estimated the value of the coefficient of restitution (e) and deviation (σ) between the theoretically derived and observed leading edge speed of the CMEs which is shown in Figure 9. From this figure, we note the probability of 72.7% for inelastic nature of collision. The probability of a super-elastic collision is around 27% and corresponds to an approaching speed ranging between 0 and $285\,\mathrm{km\,s^{-1}}$. For these super-elastic collisions, the value of σ is not larger than its value for an inelastic collision. Therefore, the values of $e > 1$ are reliable. Among all the values of e for a super-elastic collision, around 96% of them correspond to larger values of the sum of the expansion speeds of the two CMEs than their approaching speed before the collision. Around 98% of these values of e are associated with a larger expansion speed of CME2 than that of CME1 before the collision. We note that only around 45% of all the values of $e < 1$ have larger expansion speeds for CME2 than CME1.

We found that 1% of all the values of $e < 1$ correspond to a ratio of CME2 to CME1 expansion speed of around 5, however, around 12% of all the values of $e > 1$ satisfy this speed ratio. This suggests that as the ratio of expansion speed of CME2 to CME1 increases, the probability of a super-elastic collision increases compared with an inelastic one. The blank spaces at the corners in the images correspond to the values that do not satisfy the collision condition, as described in Section 3.2. From the figure, the values of e with negative approaching speed correspond to significantly larger values of σ and therefore are not reliable. Negative approaching speed implies that collision of CMEs took place because of their larger expansion speeds. The left panels of Figures 8 and 9 show that the decrease in the approaching speed increases the probability of a super-elastic collision for the selected CMEs. This finding is consistent with the concept highlighted in Shen et al. (2016).

As the larger expansion speed and internal pressure also imply a harder CME, we assume that collision tends to be super-elastic if a following CME is harder than the preceding CME. A super-elastic nature of collision has been noticed in experiments where hard ceramic spheres impact a softer polycarbonate plate (Louge & Adams 2002; Kuninaka & Hayakawa 2004). We suggest that the internal pressure of a CME indirectly stands for the physical nature of the macroscopic expanding plasma blobs. Therefore, the different physical characteristics of the CME plasma may give a different nature of collision.

4. DISCUSSION

Our analysis shows that the nature of collision of 2013 October 25 CMEs is inelastic. There also exist a smaller probability of a super-elastic collision when uncertainties of angular width, expansion speed, and initial speed of the CMEs are considered. Inelastic collision implies that some energy of the colliding CMEs is lost instead of converting to kinetic energy. This may be due to deformation, compression, and friction inside and over the colliding surface of the system, which contribute to conversion of some energy into heat. In our study, there are several idealistic assumptions which may no longer be valid in the real scenario. We have estimated the pre- and post-collision speed of the CMEs by marking the start and end of the collision phase. However, the exchange in the momentum of the CMEs might have started before the noticed collision (Temmer et al. 2012; Temmer & Nitta 2015) because of change in the local environment for CME2 and may have driven the shock of CME2 which may be passing through CME1. The role of shock in a CME–CME interaction has yet to be understood properly (Lugaz et al. 2005). A fast-mode shock may dissipate its kinetic energy into thermal and magnetic energy. Thus, ignoring the shock during the interaction probably leads to an underestimation of the nature of the collision of the two main bodies of the CMEs. Another limitation of our study is the lack of consideration of momentum exchange between the CMEs and solar wind during the collision. For the collision of two relatively slow CMEs in Shen et al. (2012), it has been shown that the acceleration of a preceding CME due to solar wind was only about 6.5% of that caused by the collision. In that study, the influence of solar wind on the following CME should have been even smaller as its speed was closer to the solar wind speed than that of the preceding CME. For the case in our study, the speed of the preceding CME is close to the slow speed ambient solar wind, but the second CME was extremely

fast. Thus, the difference in the pre- and post-collision speeds of the CMEs may not be completely attributed to the collision. Thus, the system of both the CMEs would not behave as a close system for which the conservation of momentum needs to be satisfied over the collision duration of a few hours. This is also a reason why the theoretically estimated speed is not equal to the measured post-collision speed for the CMEs.

Further, the identification of the collision phase based on the estimated kinematics of only a portion of leading edges of the CMEs creates some uncertainty in our analysis. As per our definition of collision phase, the marked start time of collision is slightly postponed compared with the actual start time where the trailing edge of CME1 is hit by the leading edge of CME2. This causes the value of the coefficient of restitution to be overestimated. The extent of overestimation depends on the deceleration of CME2 during the time of transporting the disturbance from the trailing edge to the leading edge of CME1. Based on the visual inspection of CMEs images, CME2 touches the trailing edge of CME1 around 18:00 UT on October 25. Thus, the marked start time of collision is postponed by 5 hr and CME2's leading edge speed is underestimated by 225 km s^{-1}. This finding roughly results in the overestimation of the coefficient of restitution by 50% in our study. On the other hand, an underestimation of the coefficient of restitution is also inferred because we ignored the contribution of shock to the acceleration of CME1. It will be worth investigating the effect of these two sources of error competitively causing the overestimation and underestimation of the value of the coefficient of restitution. Thus, the difficulty in marking the collision phase introduces errors into the pre- and post-collision speeds of the CMEs, however, its effect on the estimated coefficient of restitution has not been considered rigorously in our study.

We have also estimated the masses of the CMEs in coronagraphic field of view and assume that they remain the same at the collision site in the HI1 field of view (Carley et al. 2012; Bein et al. 2013). However, DeForest et al. (2013) have considered the snowplow effect in the solar wind and have shown that the mass of a CME may increase by a factor of two to three in the heliosphere. Such an increase in the mass will change the magnitude of momentum exchange of the CMEs because of their interaction with the solar wind which is ignored in our study. We further assume that the total mass of both the CMEs participates in the collision picture. In calculating the leading edges and expansion speeds of the CMEs, we have assumed the CMEs are circular structures in the ecliptic plane. This assumption may not necessarily be true but it eases our analysis. Further, the angular width of this circular structure is determined based on the GCS modeled width and orientation of the flux rope of the CME. Our analysis of these selected CMEs quite matches the diagram (Figure 4(d)) in Shen et al. (2016). The initial speed of the first CME is 485 km s^{-1}, which requires the initial approaching speed of the two CMEs to be less than 500 km s^{-1} for a super-elastic process. However, the initial approaching speed of the two CMEs is about 515 km s^{-1}, higher than 500 km s^{-1}, so the collision is inelastic or has a greater probability of being inelastic.

In analysis presented in Section 3.2.1, an arbitrary uncertainty in the direction is not directly used to estimate the change in the CME speed from the SSE method. However, the speed profiles from the SSE method having the same elongation profile is more or less independent of the direction at low elongation angle where collision occurs in our case (Howard 2011; Mishra et al. 2014). This is also evident from the extremely small error bars in Figure 3. The error in speed because of not using the SSE method with a change in direction is much less than the possible errors in speed from other sources, such as deciding the boundary of collision phase, shock–CME interaction, and drag forces on the CMEs. The effect of errors in the speed is separately dealt with in our study. Moreover, the uncertainties in the directions of the CMEs is taken in the step of $\pm 1^{\circ}$, hence repeating the SSE method hundreds of times appears impractical and futile in the context of the present study. However, we did not completely overlook the interrelatedness of direction and speed. The change in direction is considered with a change in the value of $\alpha 1$ and $\alpha 2$ in Equation (2) which will eventually modify the originally observed speed to be taken for our analysis. Thus, indirectly we are taking into account the altered speed because of the change in the direction. Similarly, the deflected direction of the CMEs is not used in the SSE method to derive their post-collision speeds. For the CMEs, a change in the direction would give new elongation profiles for the observer. Thus, the measured elongation angles and direction of propagation of CMEs are also linked. Since we are using a fixed track of elongation from the *J*-map, such an effect of direction on the kinematics is difficult to explore in a true sense. Succinctly, our analysis represents the uncertainty in the results due to observational error for a single parameter at a time. Such analysis could be considered a case study for CMEs similar to the 2013 October CMEs having only one parameter different.

We considered no change in the morphology and angular width of the CMEs during collision, and only the linear speed of their centroids was used to calculate the change in their kinetic energy as it is difficult to estimate the extent of compression and possible rotation or deflection of the CMEs during the collision. One of the major limitations of our study is that we completely ignore the magnetic field configuration of the CMEs. However, using a numerical simulation, Lugaz et al. (2013) have explored the role of the relative orientation of the magnetic flux ropes in CMEs. We have considered uncertainty in the individual parameters singly, however, uncertainty in several parameters needs to be considered together to assess the reliability of the estimated value of the coefficient of restitution. We are unable to provide any information on the physical processes during the collision, however, our study suggests that the expansion speeds of the CMEs play a role in deciding the nature of collision. The change in the angular width of the CMEs directly reflects the change in the expansion speed of the CME (Gopalswamy et al. 2009). The expansion speed of the CME is due to its larger internal pressure compared with the ambient medium (Wang et al. 2009). Hence, we believe that a following CME having a larger internal pressure leads to a super-elastic collision if it hits the preceding CME with a lower internal pressure. This may be due to the dissipation of magnetic and thermal pressure of the CME2 into kinetic energy. The change in the contact area of CMEs with different separation angles, i.e., different longitudes, may also partially contribute to deciding the nature of collision. However, with the error in direction leading to an error in the speed, this could not be confirmed from our analysis. Several case studies of colliding CMEs, including the cases analyzed previously (Lugaz et al. 2012;

Mishra & Srivastava 2014; Colaninno & Vourlidas 2015; Mishra et al. 2015a), are needed to investigate the role of duration of collision, contact area, and their expansion speeds in converting the internal magnetic or thermal energy into kinetic energy. We also note that considered uncertainties in angular width, speed, and propagation direction of the CMEs also modify the distance of collision site. It is imperative to examine the effect of collision distance on the nature of colliding CMEs. For this, in another study, we are looking at several cases of interacting CMEs wherein some are colliding close to and some away from the Sun.

There is a great scope of such studies toward the practical purpose of space weather forecasting. We think that the role of compression and subsequent expansion of CMEs and thermodynamic changes inside the CMEs during the collision phase must be well explored. We opine that elastic or super-elastic collision is not possible unless some physical processes during the collision convert magnetic or thermal energy of the CMEs to kinetic energy. These processes, such as magnetic reconnection, may be crucial in increasing the post-collision macroscopic dynamics of the CMEs. In an earlier study (Mishra & Srivastava 2014), we have shown possible signatures of magnetic reconnection in the in situ observations as a result of CME–CME interaction. Therefore, the role of magnetic reconnection in producing additional kinetic energy in the system and in deciding the type of in situ structure of both CMEs needs to be investigated. Thus, the relative orientation of the magnetic flux rope of the interacting CMEs may influence the nature of collision. The current study also highlights the drawbacks of our earlier study (Mishra & Srivastava 2014; Mishra et al. 2015a) where the expansion speed of the CME was not taken into account and a simplistic scenario of head-on collision was adopted. Although the coefficient of restitution estimated for the CMEs as per Newton's definition seems to be a fairly reasonable approach, there are three definitions for coefficient of restitution by Newton (kinematic), Poisson (kinetic), and Stronge (energetic) (Brach 1984; Stewart 2000; Lubarda 2010), we need to contemplate which definition is more suitable for the observed CMEs in a real scenario. We also plan to perform MHD simulations for the interacting CMEs following the approach described in Shen et al. (2013, 2016) to examine the consistency between observation- and simulation-based studies.

5. CONCLUSION

We have made an attempt to understand the uncertainties in the nature of the collision of magnetized expanding plasma blobs by analyzing the interacting CMEs of 2013 October 25. Our analysis suggests an inelastic nature of collision for the selected CMEs. Uncertainties in the collision nature due to the error in direction, mass, angular width, expansion, and propagation speed are examined. We show that the mass of the CMEs has almost no effect on deciding their nature of collision. Similar results have also been presented by Shen et al. (2012). We note that the head-on collision scenario causes the e value to be underestimated comapred with that of the oblique collision. For the selected CMEs, the probability of an inelastic nature of collision decreases with increasing the error in the longitude of the CMEs. The values of $e > 1$ corresponding to larger errors in longitudes lead to larger inconsistency with observed dynamics of the CMEs and therefore seem unreliable. This made us acknowledge the pseudo-effect of propagation direction of the CMEs on their collision nature. To estimate a reliable value of e, we emphasize that error in the CME directions should be considered along with the errors in CME dynamics. Our analysis in a scenario of oblique collision clearly finds that deflection of interacting CMEs is an inevitable phenomenon.

The observed kinematics of the CMEs and their angular half-width ranging between 5° and 35° results in a probability of around 75.6% for an inelastic nature of collision. The collision nature is found to be super-elastic when the ratio of CME2 to CME1 angular half-width is greater than or equal to 1.5. We also noted a super-elastic collision when the expansion speed of CME2 is greater than or equal to two times the expansion speed of CME1. We found that the lower approaching speed of the CMEs results in a greater probability of a super-elastic collision. Further, an uncertainty of 100 km s^{-1} in the initial speed of the CMEs together with the variation of their angular half-width from 5° to 35° leads to a probability of 72.7% for an inelastic nature of collision. From our analysis, we establish a concept that the larger expansion speed of CME2 compared with that of CME1, and larger values of their sum over the CME approaching speeds, tends to increase the probability of a super-elastic collision (Shen et al. 2012, 2016). We conclude that if the expansion speed of the following CME2 is larger than that of the preceding CME1, it gives a relatively low approaching speed before the collision and a relatively high separation speed after the collision, causing the nature of collision to be super-elastic. From our analysis for the CMEs of 2013 October, the relative expansion speed of the CMEs appears as a stronger factor than the relative approaching speed for deciding the nature of collision. Further study is needed to clearly understand the sufficient conditions for inelastic or super-elastic collisions.

We acknowledge the UK Solar System Data Center for providing the processed Level-2 *STEREO*/HI data. The work is supported by the NSFC grant Nos. 41131065, 41574165, and 41421063. We also thank the reviewer whose comments have greatly improved this paper. W.M. is supported by the Chinese Academy of Sciences (CAS) President's International Fellowship Initiative (PIFI) grant No. 2015PE015.

REFERENCES

Bein, B. M., Temmer, M., Vourlidas, A., Veronig, A. M., & Utz, D. 2013, ApJ, 768, 31
Brach, R. M. 1984, JAM, 51, 164
Brueckner, G. E., Howard, R. A., Koomen, M. J., et al. 1995, SoPh, 162, 357
Burlaga, L. F., Behannon, K. W., & Klein, L. W. 1987, JGR, 92, 5725
Carley, E. P., McAteer, R. T. J., & Gallagher, P. T. 2012, ApJ, 752, 36
Colaninno, R. C., & Vourlidas, A. 2009, ApJ, 698, 852
Colaninno, R. C., & Vourlidas, A. 2015, ApJ, 815, 70
Davies, J. A., Harrison, R. A., Perry, C. H., et al. 2012, ApJ, 750, 23
Davies, J. A., Harrison, R. A., Rouillard, A. P., et al. 2009, GeoRL, 36, 2102
Davies, J. A., Perry, C. H., Trines, R. M. G. M., et al. 2013, ApJL, 777, 167
DeForest, C. E., Howard, T. A., & McComas, D. J. 2013, ApJ, 769, 43
Ding, L.-G., Li, G., Jiang, Y., et al. 2014, ApJL, 793, L35
Dungey, J. W. 1961, PhRvL, 6, 47
Farrugia, C., & Berdichevsky, D. 2004, AnGeo, 22, 3679
Farrugia, C. J., Jordanova, V. K., Thomsen, M. F., et al. 2006, JGR, 111, 11104
Gonzalez, W. D., Joselyn, J. A., Kamide, Y., et al. 1994, JGR, 99, 5771
Gonzalez-Esparza, A., Santillán, A., & Ferrer, J. 2004, AnGeo, 22, 3741
Gopalswamy, N., Dal Lago, A., Yashiro, S., & Akiyama, S. 2009, CEAB, 33, 115
Gopalswamy, N., Yashiro, S., Kaiser, M. L., Howard, R. A., & Bougeret, J.-L. 2001, ApJL, 548, L91
Gosling, J. T. 1993, JGR, 98, 18937

Harrison, R. A., Davies, J. A., Möstl, C., et al. 2012, ApJ, 750, 45
Howard, T. A. 2011, JASTP, 73, 1242
Howard, T. A., & Tappin, S. J. 2009, SSRv, 147, 31
Intriligator, D. S. 1976, SSRv, 19, 629
Kaiser, M. L., Kucera, T. A., Davila, J. M., et al. 2008, SSRv, 136, 5
Kuninaka, H., & Hayakawa, H. 2004, PhRvL, 93, 154301
Liu, Y. D., Luhmann, J. G., Lugaz, N., et al. 2013, ApJ, 769, 45
Liu, Y. D., Luhmann, J. G., Möstl, C., et al. 2012, ApJL, 746, L15
Louge, M. Y., & Adams, M. E. 2002, PhRvE, 65, 021303
Lubarda, V. A. 2010, JAM, 77, 011006
Lugaz, N., & Farrugia, C. J. 2014, GeoRL, 41, 769
Lugaz, N., Farrugia, C. J., Davies, J. A., et al. 2012, ApJ, 759, 68
Lugaz, N., Farrugia, C. J., Manchester, W. B., IV, & Schwadron, N. 2013, ApJ, 778, 20
Lugaz, N., Farrugia, C. J., Smith, C. W., & Paulson, K. 2015, JGRA, 120, 2409
Lugaz, N., Manchester, W. B., IV, & Gombosi, T. I. 2005, ApJ, 634, 651
Lugaz, N., Vourlidas, A., & Roussev, I. I. 2009, AnGeo, 27, 3479
Martínez Oliveros, J. C., Raftery, C. L., Bain, H. M., et al. 2012, ApJ, 748, 66
Mishra, W., & Srivastava, N. 2014, ApJ, 794, 64
Mishra, W., Srivastava, N., & Chakrabarty, D. 2015a, SoPh, 290, 527
Mishra, W., Srivastava, N., & Davies, J. A. 2014, ApJ, 784, 135
Mishra, W., Srivastava, N., & Singh, T. 2015b, JGRA, 120, 10221
Möstl, C., Farrugia, C. J., Kilpua, E. K. J., et al. 2012, ApJ, 758, 10
Newton, I. 1687, Philosophiae Naturalis Principia Mathematica. Auctore Js. Newton (London: Jussu Societatis Regiae ac Typis Josephi Streater, Prostat apud plures Bibliopolas)
Niembro, T., Cantó, J., Lara, A., & González, R. F. 2015, ApJ, 811, 69
Rouillard, A. P., Davies, J. A., Forsyth, R. J., et al. 2008, GeoRL, 35, 10110
Schmidt, J., & Cargill, P. 2004, AnGeo, 22, 2245
Sheeley, N. R., Walters, J. H., Wang, Y.-M., & Howard, R. A. 1999, JGR, 104, 24739
Shen, C., Wang, Y., Wang, S., et al. 2012, NatPh, 8, 923
Shen, F., Shen, C., Wang, Y., Feng, X., & Xiang, C. 2013, GeoRL, 40, 1457
Shen, F., Shen, C., Zhang, J., et al. 2014, JGRA, 119, 7128
Shen, F., Wang, Y., Shen, C., & Feng, X. 2016, NatSR, 6, 19576
Stewart, D. E. 2000, SIAMR, 42, 3
Temmer, M., & Nitta, N. V. 2015, SoPh, 290, 919
Temmer, M., Vršnak, B., Rollett, T., et al. 2012, ApJ, 749, 57
Thernisien, A., Vourlidas, A., & Howard, R. A. 2009, SoPh, 256, 111
Vandas, M., Fischer, S., Dryer, M., et al. 1997, JGR, 102, 22295
Vandas, M., & Odstrcil, D. 2004, A&A, 415, 755
Vemareddy, P., & Mishra, W. 2015, ApJ, 814, 59
Wang, Y., Zhang, J., & Shen, C. 2009, JGRA, 114, A10104
Wang, Y., Zheng, H., Wang, S., & Ye, P. 2005, A&A, 434, 309
Wang, Y. M., Ye, P. Z., Wang, S., & Xue, X. H. 2003, GeoRL, 30, 1700
Webb, D. F., Möstl, C., Jackson, B. V., et al. 2013, SoPh, 285, 317
Wood, B. E., Howard, R. A., & Socker, D. G. 2010, ApJ, 715, 1524
Xiong, M., Zheng, H., & Wang, S. 2009, JGRA, 114, 11101
Xiong, M., Zheng, H., Wang, Y., & Wang, S. 2006, JGRA, 111, 11102
Xiong, M., Zheng, H., Wu, S. T., Wang, Y., & Wang, S. 2007, JGRA, 112, 11103